Hindawi
Advances in Materials Science and Engineering
Volume 2023, Article ID 9858302, 1 page
https://doi.org/10.1155/2023/9858302

Retraction

Retracted: A Performance of a Nanofiber Polymer in Geotechnical Engineering Support

Advances in Materials Science and Engineering

Received 26 December 2023; Accepted 26 December 2023; Published 29 December 2023

This article has been retracted by Hindawi, as publisher, following an investigation undertaken by the publisher [1]. This investigation has uncovered evidence of systematic manipulation of the publication and peer-review process. We cannot, therefore, vouch for the reliability or integrity of this article.

Please note that this notice is intended solely to alert readers that the peer-review process of this article has been compromised.

Wiley and Hindawi regret that the usual quality checks did not identify these issues before publication and have since put additional measures in place to safeguard research integrity.

We wish to credit our Research Integrity and Research Publishing teams and anonymous and named external researchers and research integrity experts for contributing to this investigation.

The corresponding author, as the representative of all authors, has been given the opportunity to register their agreement or disagreement to this retraction. We have kept a record of any response received.

References

[1] Y. Liu and H. Chen, "A Performance of a Nanofiber Polymer in Geotechnical Engineering Support," *Advances in Materials Science and Engineering*, vol. 2022, Article ID 5695487, 12 pages, 2022.

Hindawi
Advances in Materials Science and Engineering
Volume 2022, Article ID 5695487, 12 pages
https://doi.org/10.1155/2022/5695487

Research Article

A Performance of a Nanofiber Polymer in Geotechnical Engineering Support

Yang Liu [1] **and Haiyu Chen** [2]

[1]*School of Civil Engineering, Central South University, Changsha 410075, China*
[2]*School of Civil Engineering and Architecture, Hubei University of Arts and Science, Xiangyang 441053, Hubei, China*

Correspondence should be addressed to Haiyu Chen; hychen@hbuas.edu.cn

Received 12 May 2022; Revised 7 June 2022; Accepted 17 June 2022; Published 1 July 2022

Academic Editor: Haichang Zhang

Geotechnical engineering is a new technical system established by European and American countries in the practice of civil engineering in the 1960s. There are many methods to manufacture nanofibers, such as stretching, template synthesis, self-assembly, microphase separation, and electrospinning. Among them, electrospinning is widely used because of its simple operation, wide application range, and relatively high production efficiency. This paper aims to study how to analyze and study the properties of engineering scaffolds along the way based on nanofiber polymers. In this paper, the performance of geotechnical scaffolds is proposed, which is based on nanofibers. This paper focuses on the concept of nanofibers and geotechnical physical mechanics. In this paper, the performance of geotechnical support is designed and analyzed. The experimental results show that the initial thermal decomposition temperature of the pure SF collagen nanofiber membrane is about 250°C and that of the pure PLLA nanofiber membrane is about 330°C. When SF collagen/PLLA = 70 : 30, the initial thermal decomposition temperature of the material is about 260°C. When the mass ratio is 50 : 50, the initial thermal decomposition temperature increases to about 270°C. When the mass ratio is 30 : 70, the initial thermal decomposition temperature increases to about 280°C. This is because PLLA is a semi-crystalline polymer with certain thermal stability. Its heat resistance is better than that of pure SF collagen. With the increase in the amount of PLLA, it can effectively improve the thermal stability of blended composite nanofiber scaffolds.

1. Introduction

Geotechnical engineering is the research object to solve geotechnical engineering problems, including mechanical foundation and foundation, inclined, and underground engineering. Various types of aboveground, underground, and water projects are collectively referred to as civil engineering. Civil engineering includes stone and soil. The part of soil and water is called geotechnical engineering. There are many preparation methods of nanofibers, such as stretching, template synthesis, self-assembly, microphase separation, and electrospinning. Among them, electrospinning is widely used because of its simple operation, wide application range, and high production efficiency [1].

So far, there are many problems in various geotechnical scaffold materials in the market, such as the speed of degradation and tissue formation cannot be coordinated and combined, and it is difficult for cells to adhere and grow on the scaffold. The mechanical strength does not match the tissue, and the degradation products will lead to rejection in vivo. At the same time, it should also be noted that architecture and civil engineering is a traditional technical field with "quality first." Any fiber quality problem may cause huge losses in the reconstruction of structures. In this paper, the electrospinning method of nanofibers for the construction of geotechnical engineering scaffolds is studied and developed, which provides a more effective shortcut for the application and rapid development of nanofibers.

The innovations of this paper are as follows: (1) this paper combines nanofibers with geotechnical engineering scaffolds and introduces the theory and related methods of electrospinning technology in detail. (2) In the face of the

performance of geotechnical support, this paper analyzes and classifies the tensile performance and the thermogravimetric performance, respectively. Through the evaluation of the experimental results, this paper compares the performance of the two. This paper comes to the conclusion that the SF collagen/PLLA fiber scaffold has certain mechanical properties, but the material has strong rigidity and poor elasticity.

2. Related Work

Electrospinning technology has unique advantages in the synthesis of one-dimensional nano materials. Compared with the traditional synthesis methods of one-dimensional nano materials, electrospinning technology has incomparable advantages. Eid et al. successfully prepared hematite nanotubes by electrospinning technology and studied them by the magnetic measurement of the superconducting quantum interference device. At room temperature, the hysteresis he observed was strongly controlled by the size of nanofibers, which led to additional Morin transitions at low temperatures. However, his data is less [2]. Xiang et al. prepared one-dimensional Cu-TiO_2 nanofibers by the ionization method and used to remove phage F2. The results show that the optimum doping ratio and calcination temperature of Cu-TiO_2 nanofibers are n (Cu): n (Ti) = 1 : 8 and 450, respectively. However, his practicability is not strong [3]. He et al. briefly reviewed the basic principle and research progress of electrospinning technology (NFES). He summarized the process parameters, polymer materials, primary fiber structure, improved equipment, and potential applications of NFES. Finally, he looked forward to the development trend and challenges of NFES in the future. However, his content is not novel enough [4]. Zhang M had conducted a comprehensive survey of the strategies used to make functional fiber nanostructures. He introduced in detail the strategy to promote the better dispersion of NBBS in electrospun nanofibers. He also proposed some effective processing ways to increase the fixed sites of measured biomolecules. He discussed the applicability of electrospun nanostructures to biosensors and the advantages and disadvantages of various methods to the improve biosensor performance. However, its application scope is limited [5]. Patil et al. introduced various types of ES technologies and their technical details. He summarized the advantages and disadvantages of each ES technology. It covers a clear literature survey on the growth of various metal oxide nanostructures and their applications in different fields. In addition, he also discussed the future prospects. However, his research focus is not prominent enough [6]. Gelatin, zein, and gelatin/zein films in Deng et al. study were manufactured by electrospinning and solvent casting, respectively. He performed scanning electron microscopy, differential scanning calorimetry, Fourier transform infrared spectroscopy, and water contact angle measurements to characterize the morphology, molecular interaction, thermal behavior, and surface hydrophilicity of electrospun and cast films. The results showed that zein particles prevented the intramolecular aggregation of gelatin chains in the casting film due to uneven mixing, while strong hydrogen bonds were formed in the nanofiber film due to uniform mixing. However, his process is more complex [7]. Topuz and Uyar showed the electroplating of gelatin and studied it in detail. Its fiber morphology ranges from round to flat/banded. He correlated the fiber morphology with its parameters, electroplating process, and gelatin concentration in electroplating solution. His analysis showed that after the electrospinning process, the triple helix crystal structure in gelatin was lost. However, his influencing factors are not single [8]. Cui et al. reported a simple and controllable electrospinning technology. Polyvinylidene fluoride (PVDF)/stearic acid (SA) nanofibers can be prepared on metal substrates in order to achieve long-term corrosion protection. The electrochemical corrosion test results show that the superhydrophobic PVDF/SA nanofiber coating still has an excellent long-term corrosion resistance of metal substrate even after soaking in 3.5 wt% NaCl aqueous solution for 30 days. However, his performance is not high [9].

3. Methods of Geotechnical Support

3.1. Physical and Mechanical Parameters of Rock and Soil

3.1.1. Experiment on Physical and Mechanical Parameters of Rock and Soil

(1) Uniaxial Compressive Strength. The uniaxial compressive strength of rock is actually the final bearing capacity of the sample under uniaxial pressure, and its size is the maximum stress of the sample when it is destroyed [10]. The uniaxial stress resistance can be expressed by the ratio of the maximum axial force Q experienced by the sample at the time of failure to the cross-sectional area a of the test sample, that is, the uniaxial compressive strength T_c.

$$T_c = \frac{Q}{A}. \tag{1}$$

Among them, the compressive strength is expressed as T_c (MPA), the maximum load is expressed as Q (MN), and the cross-sectional area of the specimen perpendicular to the axial load is expressed as a (M^2).

(2) Uniaxial Tensile Strength. The uniaxial tensile strength of rock is actually the maximum bearing capacity that the specimen can bear under the influence of uniaxial tension, and its size is actually equal to the maximum tensile stress when the specimen is damaged. The tensile strength can be calculated by the following formula:

$$T_k = \frac{2p}{\pi Dl}. \tag{2}$$

Among them, the tensile strength is expressed as T_k (MPA), the final pressure when the specimen fails is expressed as Q (MN), the diameter of the cylindrical specimen is expressed as D (mm), and the length is expressed as l (mm).

Table 1: Physical and mechanical parameters of roof and floor.

Rock formation name	Shear modulus G/GPa	Tensile strength k/MPa	Bulk modulus V/GPa	Density d/N·m^3	Adhesion c/MPa	Friction angle f/°
Laodi	1.78	3.6	2.19	2380	5.45	39.9
Direct bottom	2.12	3.l	2.42	2510	5.51	38.4
Coal seam	0.81	1.6	1.48	1340	2.53	36.4
Direct top	2.2	2.6	2.41	2490	5.57	38.3
Basic top	3.6	3.2	4.1	2520	6.29	39

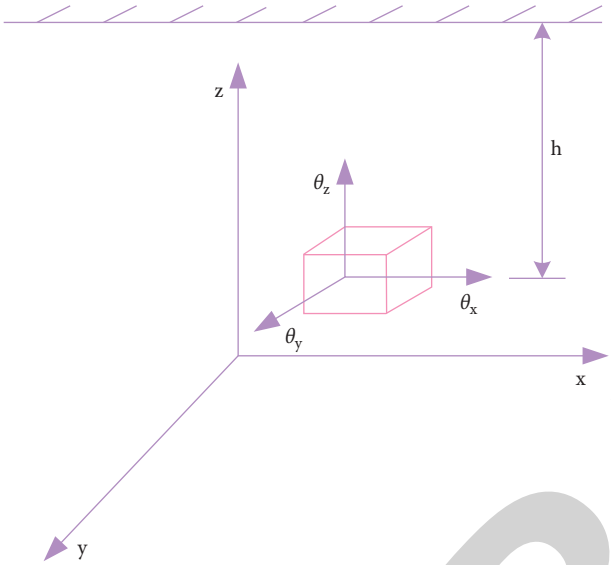

Figure 1: Gravity vertical stress of the rock mass.

(3) Uniaxial Shear Strength. The shear test of rock is usually carried out with different β values. It is pressurized on the press until shear failure occurs. In the uniaxial shear test of rock, the normal stress θ and shear stress ε generated on the shear plane can be obtained by the following formula:

$$\theta = \frac{Q}{A}(\cos\beta + f\sin\beta),$$
$$\varepsilon = \frac{Q}{A}(\cos\beta - f\sin\beta). \quad (3)$$

Among them, the maximum load applied on the press is expressed as Q (MN), the friction coefficient of the ball is expressed as F, the surface area of shear failure is expressed as A (M^2), and the angle between the shear plane and the horizontal plane is expressed as β (°).

3.1.2. Determination of Mechanical Parameters of the Coal and Rock Mass. The physical and mechanical parameters of the coal and rock mass obtained from the above experiments and the calculation relationship of relevant parameters are shown in Table 1.

3.1.3. Calculation of Initial In-Situ Stress and Surrounding Rock Pressure of Surrounding Rock. The initial and boundary conditions of the numerical calculation model of the advance roadway and the similar physical test model in the laboratory need to be based on the initial in-situ stress and pressure of surrounding rock. The support strength of advanced hydraulic support shall be determined based on the surrounding rock pressure borne by support under the most dangerous working conditions [11, 12]. Therefore, it is of great significance to calculate the initial in-situ stress and surrounding rock pressure of surrounding rock.

(1) Calculation of Initial In-Situ Stress of Surrounding Rock. Generally speaking, in-situ stress refers to the original rock stress that the rock mass is not disturbed by mining. The vertical voltage and horizontal voltage of the rock mass are generated by the self-weight voltage of the rock mass [13]. Assuming that a unit body is selected from the surface depth h as the investigation object, as shown in Figure 1. It is generally assumed that the self-weight of the rock mass at underground depth is h, the vertical voltage generated at this point must be the weight of the unit body ⊥ overburden rock mass, i.e.,

$$\theta_z = \lambda h. \quad (4)$$

Among them, ⊥ the average weight of the overburden rock mass is expressed as λ (25 kN/m^3); the depth of the rock mass unit is h (528m).

Substituting these parameters, we get

$$\theta_z = 25 \times 528 = 13.2MPa. \quad (5)$$

The rock mass is generally regarded as isotropic elastomer, and each direction of the unit body in the rock mass will be limited by other adjacent units, so the unit body cannot deform laterally, that is,

$$\phi_x = \phi_y = 0. \quad (6)$$

The surrounding rock limit of the unit body is equivalent to the DF trend stresses θ_x and θ_y of the surrounding rock and the unit body. According to Hooke's general law, there are

$$\phi_x = \frac{1}{E}\left[\theta_x - \alpha\left(\theta_y - \theta_z\right)\right] = 0,$$
$$\phi_y = \frac{1}{E}\left[\theta_y - \alpha\left(\theta_z - \theta_x\right)\right] = 0. \quad (7)$$

This leads to

$$\theta_x = \theta_y = \frac{\alpha}{1-\alpha}\theta_z = \frac{\alpha}{1-\alpha}\lambda Z. \quad (8)$$

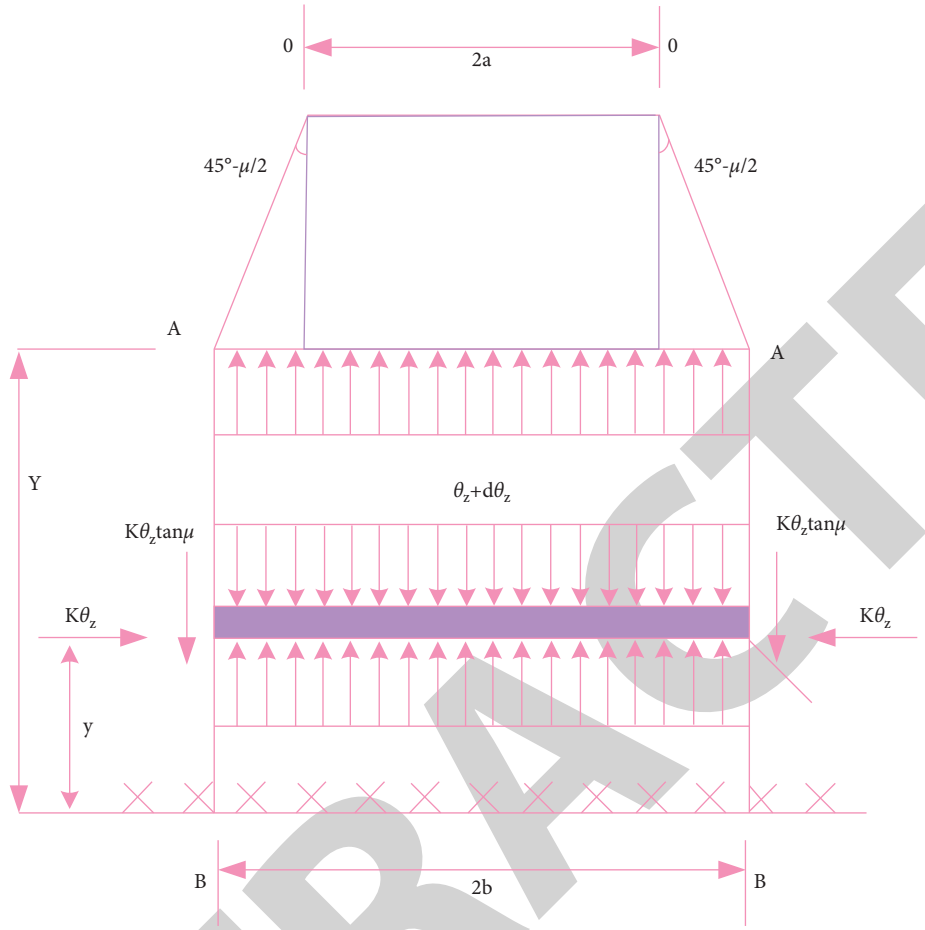

Figure 2: Calculation diagram of surrounding rock pressure.

Among them, the Poisson's ratio of the rock mass is expressed as α, and the value is 0.25.

Substituting these parameters, we get

$$\theta_x = \theta_y = \frac{0.25}{1-0.25} \times 25 \times 528 = 4.4MPa. \quad (9)$$

(2) Calculation of Surrounding Rock Pressure. The pressure of surrounding rock is mainly due to the destruction of the tension balance state of the original rock after road excavation, resulting in the redistribution of the tension of surrounding rock. According to the concept of loose surrounding rock pressure, the weight of the rock mass damaged in a certain range around the roadway is generally equal to this force. That is, the weight of the rock mass within a certain failure range is equal to the vertical stress acting on the support system. In order to determine the surrounding rock pressure acting on the supporting structure, according to the concept of relevant theory, the surrounding rock of the roadway is regarded as a granular body. After the roadway is excavated, the surrounding rock will form an unloading arch [14, 15], as shown in Figure 2.

It is considered that the overlying rock mass above the underground pavement gradually sinks due to pavement deformation, and the OAB dislocation surface is gradually formed in this process. When the vertical compressive stress θ_z applied to all horizontal sections is evenly distributed, the corresponding horizontal stresses θ_h and θ_z are equal to K, that is,

$$K = \theta_h/\theta_z. \quad (10)$$

Pulling out the horizontal bar with the thickness of dy from the ground depth y, and checking the balance state $\sum V = 0$ of the horizontal bar. It is concluded that

$$\frac{d\theta_z}{(\lambda - K\theta_z \tan\mu/b)} - dy = 0. \quad (11)$$

Among them, the similar friction angle of surrounding rock is expressed as μ (36.49°), $\perp$ the average gravity of overburden is expressed as λ (25 kn/m^3), and half of the loose width is expressed as b.

By integrating formula (10) and introducing the boundary condition $y = 0$, $\theta_z = 0$, we get

$$\theta_z = \frac{\lambda b}{K\tan\mu}\left(1 - e^{-K\tan\mu\dfrac{y}{b}}\right). \quad (12)$$

With the continuous increase of roadway buried depth y, $e^{-K\tan\mu y/b}$ in the formula will approach zero, and θ will eventually approach a fixed value, and

$$\theta = \frac{\lambda b}{K \tan \mu}. \tag{13}$$

According to the experimental results, $k = 1.0\sim1.5$, take $k = 1.0$, then

$$\theta = \frac{\lambda b}{\tan \mu}. \tag{14}$$

It is known from the geometric relationship that

$$b = a + H \tan\left(45^\circ - \frac{\mu}{2}\right). \tag{15}$$

Among them, the pavement height is expressed as H (3 m), and half of the pavement width is expressed as a (2.25 m).

Substituting relevant parameters, we get

$$\theta_z = \frac{25}{\tan 36.4} \times 3.765 = 127.682k \frac{N}{m^2}. \tag{16}$$

In order to meet the support requirements under the most dangerous working conditions, considering the influence of mining in this working face and surrounding working faces, the support strength of advance support shall be taken as

$$p = k_1 k_2 \theta_z. \tag{17}$$

Among them, the mining influencing factors of the upper working face are expressed as k_1 (1.6), and the influencing factors of the working face are expressed as k_2 (2).

Substituting relevant parameters, we get

$$p = 1.6 \times 2 \times 0.12768 = 0.409MPa. \tag{18}$$

3.2. Stent

3.2.1. Principle of Advanced Hydraulic Wenchai Support. The support process of advanced hydraulic support refers to the process of mutual mechanical interaction between the self-jacking beam and base, and the top and bottom plate, which can be divided into three stages: initial support, bearing, and constant resistance [16].

(1) Initial Support Stage. In the process of lifting the hydraulic support column, when the leading hydraulic support top beam contacts the top plate, the liquid pressure in the lower cavity of the hydraulic support column will gradually increase after the top plate is affected by surrounding rock pressure. When pressure increases to set pressure, the hydraulic control check valve will be closed immediately, and the emulsion pump will no longer supply liquid to the column. This state is considered as the initial support stage of hydraulic support. At this time, the support of hydraulic support is called the initial support force of support [17], and the expression is

$$q_c = \frac{\pi}{4} \times d^2 \times n \times q_b \times 10^3. \tag{19}$$

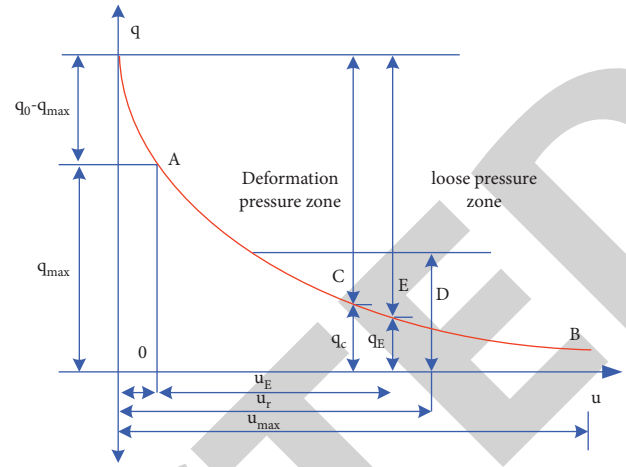

Figure 3: Schematic diagram of interaction principle.

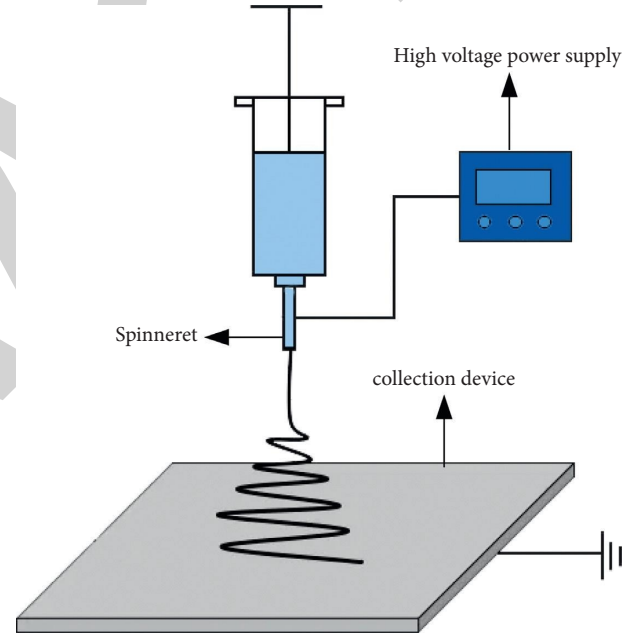

Figure 4: Schematic diagram of electrospinning.

Among them, the cylinder diameter and quantity of the support column are expressed as d, n, respectively; the working pressure of the pump station is expressed as q_b.

(2) Bearing Stage. After the initial support of advance support is completed, with the continuous mining advance of the working face, the influence of mining is becoming greater and greater. At this time, the pressure of the top plate on support will be greater and greater, and the pressure of the lower cavity of the column will be greater and greater, so the initial support force of the top beam on the top plate will also increase, showing a resistance increasing state. This process is called the bearing stage of advance hydraulic support [18, 19].

(3) Constant Resistance Stage. With increasing pressure on hydraulic support, hydraulic pressure in the lower chamber

Table 2: Common methods for preparation of geotechnical support.

Name	Definition	Advantage	Shortcoming
Electrospinning	It is a simple and effective process for obtaining nanoscale fibers by using a polymer solution to form a jet stream under high pressure for spinning processing	Similar to natural ECM, most suitable for cell migration and proliferation; scaffolds can be modified by electrospinning parameters	The fibers are denser, which is not conducive to the growth of cells
Fiber adhesion	It is to use the characteristics that two polymers have different solubility in a certain solvent and do not melt each other when heated, and one polymer is embedded in another polymer matrix, so that the polymer fibers are bonded at the intersection up to form a three-dimensional connected fiber network	Good porosity and a specific surface area can be obtained; facilitating cell adhesion and nutrient diffusion	Poor stability; strength and rigidity are low, and it is easy to cause damage to the planted cells
Pore former precipitation method	Porous scaffolds are prepared by uniformly mixing the screened particles, such as sodium chloride and citrate in a polymer solution, removing the solvent by freeze-drying or melting and casting, and the space occupied by them becomes pores	More than 93% hole team rate can be obtained; pore diameter can reach 500 μm	Uneven distribution of pores; only stents with a thickness of not more than 3 mm can be prepared
Melt molding	The polymer powder and the leachable phase are premixed uniformly, poured into an abrasive tool, heated to above the glass transition temperature of the polymer, and soaked in water after molding to remove the leachable phase to obtain a two-dimensional space scaffold with a complex structure	Pore height is regular and repeatable; the structure of the pores can be adjusted by the size and amount of the leachable phase	Heating the material during the preparation process can cause changes in the properties of the polymer, and the leachable phase is not easy to remove
...	...	...	...

Table 3: Comparison of performance characteristics of different plates.

Plate variety	High strength PP fiber	Asbestos	PVA fiber
Fiber diameter (um)	12	5	14
Cutting length (mm)	10	5	6
Dry strength (MPa)	850	3100	1600~1800
Elongation at break (%)	21	0.5	7
Young's modulus (GPa)	6	160	32~36

of the column continues to increase. The internal liquid flows outward. When pressure is lower than the set pressure value, the safety valve will close automatically again. According to the dynamic change of force on support, the process will be repeated continuously. Therefore, the supporting force of hydraulic support remains at a constant value, which is called the constant resistance stage. The force of support on the top plate is called the working resistance of support, so the working resistance of leading support is

$$q_d = \frac{\pi}{4} \times d^2 \times n \times q_a \times 10^3. \quad (20)$$

The set pressure of the safety valve is expressed as q_a.

3.2.2. Principle of "Support Surrounding Rock" Interaction. The design of the geotechnical support structure is generally based on elastic-plastic theory. Due to pavement excavation, the equilibrium state between the surrounding rock and the original rock is damaged. In order to find a new equilibrium, the stress of the surrounding rock will be redistributed. When the tension of the surrounding rock is lower than that of the surrounding rock in the new process, it can continue to be stable. The pavement around the rock will break and deform, and support must be provided immediately [20], and its schematic diagram is shown in Figure 3.

3.3. Electrospinning Technology. In the research process of nanomaterials, electrospinning technology continues to play a very important role with its outstanding technical characteristics. It is a new type of nanofiber material with a unique structure and shape [21]. By changing the structure of the capillary nozzle, we can adjust, adapt, and change various conditions of the experimental ligament, and change and combine different experimental parameters. It can

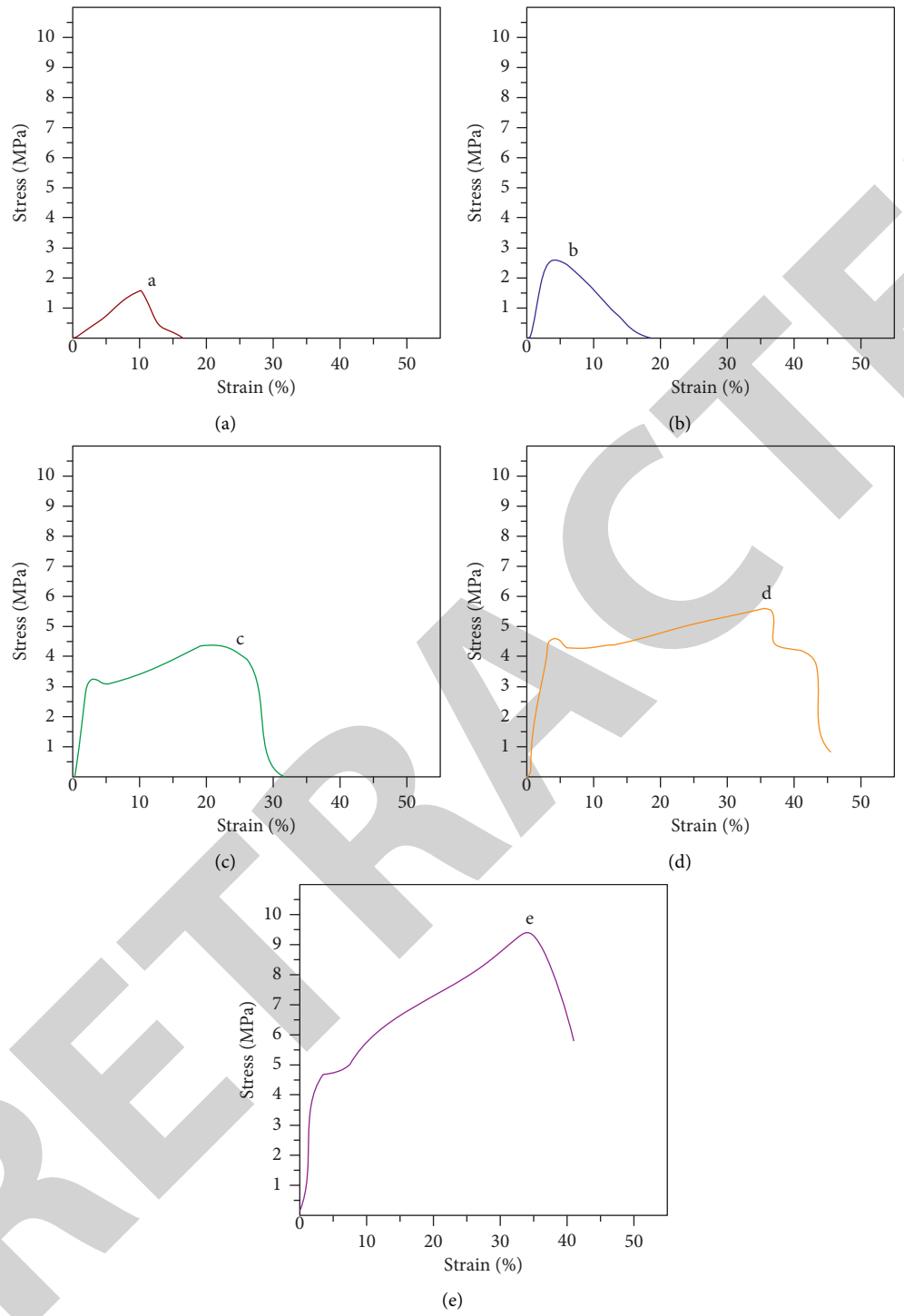

Figure 5: Tensile behavior of the SF collagen/PLLA fiber scaffold.

obtain various ultrafine fibers with three different solid, hollow, and core-shell structures. It is a three-dimensional fiber membrane material with a network structure. In addition, the structure of different fiber collection devices can be changed according to the design, and it can also be used separately, including multiple highly oriented fiber bundles and randomly oriented fiber films. However, electrospinning technology is not smooth in the adjustment and construction of the fiber structure, there are still difficulties, and the risk should not be underestimated [22].

The traditional electrospinning device consists of three parts: high voltage power supply, injection pump (including injection needle and rotating needle), and assembly device, as shown in Figure 4. The jet pump squeezes the rotating solution with specific concentration and viscosity at a constant liquid delivery speed, and forms droplets under the

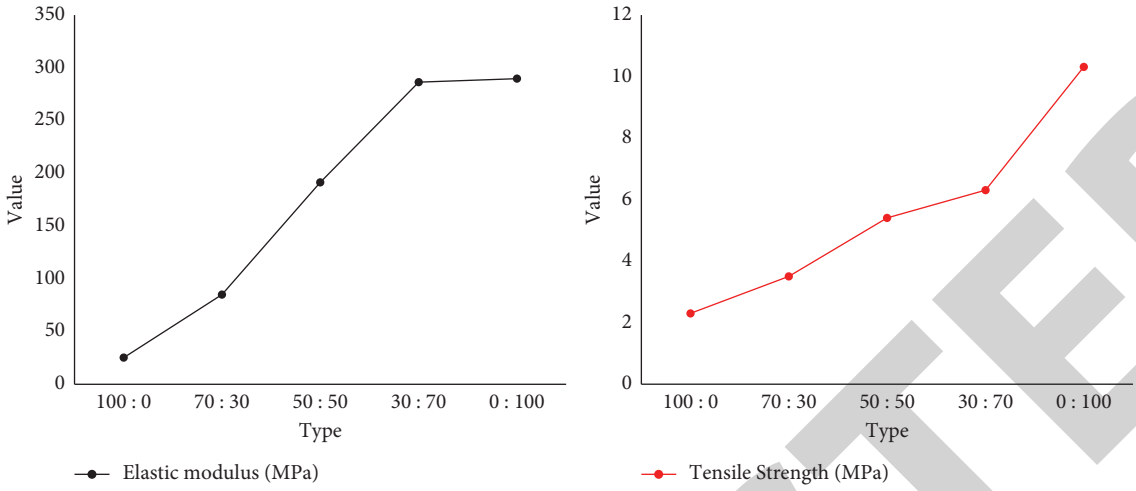

Figure 6: Tensile properties of SF collagen/PLLA fiber scaffolds.

action of surface tension. Then, these droplets form suspended droplets under the action of electrostatic repulsion and extend into the ejector. Under the action of high voltage, the thin film is rapidly solidified under the action of a transverse electric field.

In fact, the theoretical knowledge analysis of the preparation of polymer nanofibers by electrospinning is quite complex [23]. It involves many theoretical knowledge, such as turbulence, rheology, air and current volume dynamics, electrostatics, charge transport knowledge exchanged on solid-liquid surface, heat transfer, and mass transfer.

4. Performance Test and Geotechnical Support

4.1. Preparation Method of Geotechnical Support. Most of the materials used to prepare scaffolds exist in the form of solid particles, which requires a certain series of treatment before they can be used in tissue engineering [24]. Choosing the preparation method is particularly important for the scaffold because various treatment methods will lead to significant changes in the physical and chemical properties and biological activities of the prepared scaffold, such as surface shape, mechanical properties, degradation rate, and hydrophilicity. Common methods are listed in Table 2 below.

4.2. Application of Chemical Fiber in Fiber Reinforced Concrete. At present, the chemical fibers widely used in cement and concrete reinforcement mainly include polyene warp (PP or PE) fiber, polyamide (PA) fiber, polypropylene sheet (Pan) fiber, polyvinyl alcohol (PVA) fiber, and cellulose fiber.

In the research study on asbestos-free technology of cement-based composites, the research on improving fiber interface friction has achieved results [25]. Using the fiber dispersion and affinity with cement, polypropylene high-strength fiber is successfully used as the reinforcing phase of cement-based composites. So far, about 200 million square meters of polypropylene high-strength fiber reinforced cement board has been put on the market. Table 3 compares the performance characteristics of high strength PP fiber reinforced cement board with other boards.

PVA has high strength, high modulus, excellent chemical resistance, and good dimensional stability under hot and humid conditions. It has won the general recognition of consumers in the field of fiber-reinforced cement boards.

In recent years, in the field of high-performance fiber concrete, the mixing method of two or more fibers has attracted extensive attention. The research on cement-based composites shows that the hybrid fiber system can effectively improve the quality of concrete products [26, 27].

4.3. Physical and Chemical Properties of Composite Nanofiber Scaffolds

4.3.1. Tensile Property Analysis. As a tissue engineering scaffold material of bionic ECMs, its mechanical properties determine the application field. The mechanical properties of different tissues are different, but the materials are required to provide mechanical support. Next, this paper takes SF collagen/PLLA as an example.

Figure 5 shows the tensile stress-strain curve of SF collagen/PLLA fiber support.

As can be seen from Figure 5(a), the elongation at break of the pure SF collagen group is $9.89 \pm 0.19\%$, and tensile strength is very small, only 1.46 ± 0.50 MPa, showing a typical brittle fracture. It may be that SF and collagen are natural proteins, and glycine, alanine, tryptophan (short side-chain amino acids), and group amino acids (charged long side-chain amino acids) form polypeptides. The hydrogen bond and van der Waals binding force between peptides are weak and easy to be destroyed during stretching. In addition, the mechanical properties of scaffolds are not only related to the properties of prepared

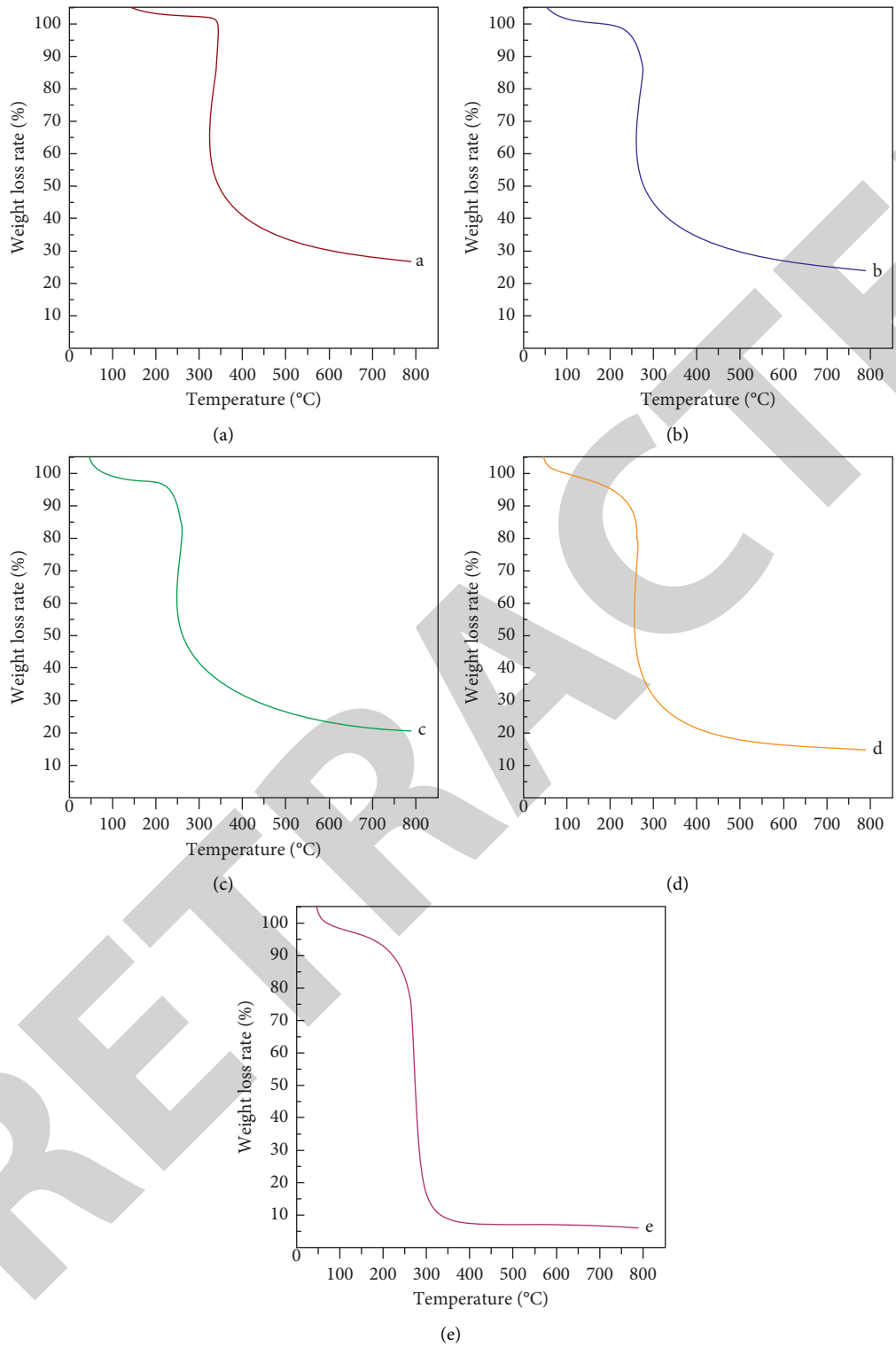

Figure 7: TG profiles of SF-collagen/PLLA composite nanofiber scaffolds.

materials, but also related to the fiber scaffold structure formed by electrospinning (such as fiber diameter, length, porosity, pore size, pore number, specific surface area, etc.).

In the experiment, it was observed that the fiber of the pure SF/collagen group was shorter than that of other groups, and the fiber scaffold formed was more loose. The tensile strength of the SF group was very similar to that of the pure collagen group when SF was added to 76.2 MPa. However, the elongation at break was only reduced to $6.13 \pm 0.35\%$ because the hydrophilicity of PLLA, SF, and

Table 4: Initial decomposition temperature of SF-collagen/PLLA composite nanofiber scaffolds.

SF-collagen/PLLA blending mass ratio	Initial decomposition temperature (°C)
0 : 100	252.3
30 : 70	261.7
50 : 50	272.2
30 : 70	284.5
0 : 100	326.0

collagen molecules were very different. After mixing, PLLA, SF, and collagen could not be dissolved in hexafluoroisopropanol, resulting in serious phase separation. In this process, SF collagen may bring the main tensile strain, leading to the early occurrence of the fracture. SF collagen played an important role in the SF collagen/PLLA group (70 : 30). When SF collagen/PLLA is (50 : 50 and 30 : 70), the stress deformation curves between the two groups are similar. There are three changes in the tensioning process of support: elastic deformation, that is, the tensile deformation of support, including small sliding between fibers. There is a small slip between the fibers, but deformation changes little and tensile strength increases little. Continuous deformation: the duration is long, but the value changes little. Fracture deformation: the fracture of the material is different from that of the pure PLLA group (*E*). Just like the fracture of the molecular chain, the tensile stress decreases sharply. Experiments show that a large number of fibers are stripped and the stress decreases slowly.

Figure 6 shows the tensile property parameters of each group of materials.

It can also be seen from Figure 6 that the elastic modulus and tensile strength of the SF collagen/PLLA fiber scaffold increase with the increase of PLLA quality. SF collagen/PLLA has large elastic modulus and small tensile elongation, which indicates that the material shows good rigidity, but the elasticity is still poor [28]. The addition of PLLA improved the brittleness of SF collagen.

4.3.2. Thermogravimetric Analysis. TG is a method to measure the weight change of materials during heating. The initial thermal decomposition temperature and the decomposition rate of materials can be analyzed through the results. Figure 7 shows the TG spectra of SF collagen/PLLA fiber scaffolds with different mass ratios. Among them, A represents 100 : 0, B represents 70 : 30, C represents 50 : 50, *D* represents 30 : 70, and *E* represents 0 : 100. As shown in Figure 7 and Table 4, the initial thermal decomposition temperature of the pure SF collagen nanofiber membrane is about 250°C, and the initial thermal decomposition temperature of the pure PLLA nanofiber membrane is about 330°C. When SF collagen/PLLA = 70 : 30, the initial thermal decomposition temperature of the material is about 260°C. When the mass ratio is 50 : 50, the initial thermal decomposition temperature increases to about 270°C. When the mass ratio is 30 : 70, the initial thermal decomposition temperature increases to about 280°C. This is because PLLA is a semi-crystalline polymer with certain thermal stability, and its heat resistance is better than that of pure SF collagen. With the increase of PLLA content, the thermal stability of blend composite nanofiber scaffolds can be effectively improved.

5. Discussion

Firstly, through the study of relevant knowledge points of literature works, this paper preliminarily mastered the relevant basic knowledge and analyzed how to study the performance of engineering scaffolds along the way based on nanofiber polymers. This paper expounds the physical mechanics of rock and soil, explores the electrospinning technology, and analyzes the applicability of the nanofiber polymer in geotechnical engineering support through experiments.

With the rapid development of nanoscience and technology, electrospinning technology is a simple and effective new nanofiber processing technology. It plays a great role in biomedical organizations and aerospace fields. The properties of inorganic and organic composite nanofibers depend on the structure of nanoparticles, the synergistic properties of nanoparticles, and the aggregation method. Many factors make it a complex system and a suitable preparation method. High-performance and multifunctional composite nanofibers have become the key problem to further study and guide the polymerization of nanofibers.

Experimental analysis shows that the pure SF collagen fiber scaffold is a typical brittle fracture. With the increase in the amount of polymer PLLA in the blend, SF collagen/PLLA fiber scaffolds possess certain mechanical properties. However, the material has strong rigidity and poor elasticity. The thermal stability of SF collagen/PLLA fiber scaffolds is higher than that of pure SF collagen, and with the increase of PLLA, the thermal stability is better.

6. Conclusion

At present, with the transformation and upgrading of China's economic structure, environmental protection has attracted more and more attention. Therefore, new requirements are put forward for industrial buildings. The rapid development of nanotechnology not only leads to the continuous improvement of scientific and technological level but also has a significant impact on the geotechnical engineering industry. In the field of geotechnical engineering disaster prevention and reduction, engineers pay more and more attention to it. The study of phase behavior and the phase structure of polymers and polymer blends is very important for both basic research and applied technology research. Although the prepared nanomaterials have made some achievements, due to the author's own level and time, there are still some deficiencies in the current research work, and the related work is still necessary to continue.

Data Availability

The data that support the findings of this study are available from the corresponding author upon reasonable request.

Conflicts of Interest

The authors declared that they have no conflicts of interest.

Acknowledgments

This work was supported by the Scientific Research Project of the Education Department of Hubei Province, China (B2021214).

References

[1] B. Zaarour and N. Mayhoub, "Effect of needle diameters on the diameter of electrospun PVDF nanofibers," *International Journal of BIM and Engineering Science*, vol. 4, no. 2, pp. 26–32, 2021.

[2] C. Eid, D. Luneau, V. Salles et al., "Magnetic properties of hematite nanotubes elaborated by electrospinning process," *Journal of Physical Chemistry C*, vol. 115, no. 36, pp. 17643–17646, 2011.

[3] X. Zheng, Z. P. Shen, C. Cheng, L. Shi, R. Cheng, and J. Dong, "Electrospinning Cu–TiO2 nanofibers used for photocatalytic disinfection of bacteriophage f2: preparation, optimization and characterization," *RSC Advances*, vol. 7, no. 82, pp. 52172–52179, 2017.

[4] X. X. He, J. Zheng, G. F. Yu et al., "Near-field electrospinning: progress and applications," *Journal of Physical Chemistry C*, vol. 121, no. 16, pp. 8663–8678, 2017.

[5] M. Zhang, X. Zhao, G. Zhang, G. Wei, and Z. Su, "Electrospinning design of functional nanostructures for biosensor applications," *Journal of Materials Chemistry B*, vol. 5, no. 9, pp. 1699–1711, 2017.

[6] J. V. Patil, S. S. Mali, A. S. Kamble, C. K. Hong, J. H. Kim, and P. S. Patil, "Electrospinning: a versatile technique for making of 1D growth of nanostructured nanofibers and its applications: an experimental approach," *Applied Surface Science*, vol. 423, pp. 641–674, 2017.

[7] L. Deng, X. Kang, Y. Liu, F. Feng, and H. Zhang, "Characterization of gelatin/zein films fabricated by electrospinning vs solvent casting," *Food Hydrocolloids*, vol. 74, pp. 324–332, 2018.

[8] F. Topuz and T. Uyar, "Electrospinning of gelatin with tunable fiber morphology from round to flat/ribbon," *Materials Science and Engineering: C*, vol. 80, pp. 371–378, 2017.

[9] M. Cui, C. Xu, Y. Shen, H. Tian, H. Feng, and J. Li, "Electrospinning superhydrophobic nanofibrous poly(vinylidene fluoride)/stearic acid coatings with excellent corrosion resistance," *Thin Solid Films*, vol. 657, pp. 88–94, 2018.

[10] H. Yu, Y. Li, X. Lan, and Z. Liang, "Electrospinning preparation and luminescence properties of La2O3:Ce3+/Tb3+ nanofibers," *Journal of Materials Science: Materials in Electronics*, vol. 28, no. 12, pp. 8832–8836, 2017.

[11] S. Yan, X. Li, J. Dai et al., "Electrospinning of PVA/sericin nanofiber and the effect on epithelial-mesenchymal transition of A549 cells," *Materials Science and Engineering: C*, vol. 79, pp. 436–444, 2017.

[12] H. Chen, A. d B. F. B. Malheiro, C. van Blitterswijk, C. Mota, P. A. Wieringa, and L. Moroni, "Direct writing electrospinning of scaffolds with multi-dimensional fiber architecture for hierarchical tissue engineering," *ACS Applied Materials & Interfaces*, vol. 9, no. 44, pp. 38187–38200, 2017.

[13] A. Tampau, C. Gonzalez-Martinez, and A. Chiralt, "Carvacrol encapsulation in starch or PCL based matrices by electrospinning," *Journal of Food Engineering*, vol. 214, pp. 245–256, 2017.

[14] S. T. Aruna, L. S. Balaji, S. S. Kumar, and B. S. Prakash, "Electrospinning in solid oxide fuel cells – a review," *Renewable and Sustainable Energy Reviews*, vol. 67, pp. 673–682, 2017.

[15] H. Gao, Y. Yang, O. Akampumuza, J. Hou, H. Zhang, and X. Qin, "A low filtration resistance three-dimensional composite membrane fabricated via free surface electrospinning for effective PM2.5 capture," *Environmental Science Nano*, vol. 4, no. 4, pp. 864–875, 2017.

[16] M. Noori, F. Ravari, and M. Ehsani, "Preparation of PVA nanofibers reinforced with magnetic graphene by electrospinning method and investigation of their degradation kinetics using master plot analyses on solid state," *Journal of Thermal Analysis and Calorimetry*, vol. 132, no. 1, pp. 397–406, 2017.

[17] J. Faria, C. Echeverria, J. P. Borges, M. H. Godinho, and P. I. P. Soares, "Towards the development of multifunctional hybrid fibrillary gels: production and optimization by colloidal electrospinning," *RSC Advances*, vol. 7, no. 77, pp. 48972–48979, 2017.

[18] N. H. A. Ngadiman, N. M. Yusof, A. Idris, E. Misran, and D. Kurniawan, "Development of highly porous biodegradable γ-Fe2O3/polyvinyl alcohol nanofiber mats using electrospinning process for biomedical application," *Materials Science and Engineering: C*, vol. 70, no. 1, pp. 520–534, 2017.

[19] J. Ju, Z. Shi, L. Fan, Y. Liang, W. Kang, and B. Cheng, "Preparation of elastomeric tree-like nanofiber membranes using thermoplastic polyurethane by one-step electrospinning," *Materials Letters*, vol. 205, pp. 190–193, 2017.

[20] T. D. Stocco, B. V. M. Rodrigues, F. R. Marciano, and A. O. Lobo, "Design of a novel electrospinning setup for the fabrication of biomimetic scaffolds for meniscus tissue engineering applications," *Materials Letters*, vol. 196, pp. 221–224, 2017.

[21] X. Xu, D. Shahsavari, and B. Karami, "On the forced mechanics of doubly-curved nanoshell," *International Journal of Engineering Science*, vol. 168, Article ID 103538, 2021.

[22] U. Ali, H. Niu, S. Aslam, A. Jabbar, A. W. Rajput, and T. Lin, "Needleless electrospinning using sprocket wheel disk spinneret," *Journal of Materials Science*, vol. 52, no. 12, pp. 7567–7577, 2017.

[23] A. A. Elngar and S. E. El-Dek, "A novel artificial face mask based nanofibers with special intelligent engineered nanocomposite against covid-19," *Journal of Cybersecurity and Information Management*, vol. 5, no. 2, pp. 21-22, 2021.

[24] Bo Gao, N. Xu, and P. Xing, "Shock wave induced nanocrystallization and its effect on mechanical properties," *Materials Letters*, vol. 237, no. 15, pp. 180–184, 2019.

[25] P. Wang, T. Yao, Z. Li et al., "A superhydrophobic/electrothermal synergistically anti-icing strategy based on graphene composite," *Composites Science and Technology*, vol. 198, Article ID 108307, 2020.

[26] Y. Kishimoto, H. Morikawa, S. Yamanaka, and Y. Tamada, "Electrospinning of silk fibroin from all aqueous solution at low concentration," *Materials Science and Engineering: C*, vol. 73, pp. 498–506, 2017.

[27] Z. Liu, K. K. J. Ang, and J. He, "Needle-disk electrospinning inspired by natural point discharge," *Journal of Materials Science*, vol. 52, no. 4, pp. 1823–1830, 2017.

[28] X. Zhang, Z. Li, X. Wang, and J. Yu, "The fractional kelvin-voigt model for circumferential guided waves in a viscoelastic fgm hollow cylinder," *Applied Mathematical Modelling*, vol. 89, pp. 299–313, 2021.